Journal of Inorganic and Organometallic Polymers and Materials (2019) 29:710–720
https://doi.org/10.1007/s10904-018-1044-z

Facile Synthesis of Ag/ZnO Photocatalysts on the Degradation of Diuron Herbicide Under Simulated Solar Light and the Investigation of Its Antibacterial Activity for Waste-Water Treatment

Mohamed Ali Saidani[1] · **Anis Fkiri**[1] · **Leila-Samia Smiri**[1]

Received: 3 September 2018 / Accepted: 6 December 2018 / Published online: 13 December 2018

Abstract

Nanocrystalline Ag/ZnO powders have been successfully prepared by a modified polyol process using triethylene-glycol (TEG) as solvent, reducing and stabilizing agent. The synthesis procedure has been conducted without any post-synthesis thermal treatment. The structural and optical properties have been characterized by X-ray diffraction, transmission electron microscopy, N2 adsorption study, inductively coupled plasma optical emission spectroscopy and UV–Vis diffuse reflectance spectroscopy. The photocatalytic activity of Ag/ZnO materials has been studied by analyzing the degradation of an herbicide, diuron, under solar light. Ag/ZnO photocatalysts with optimized x = 0.7% Ag content showed 14 times higher rate of degradation than that of unmodified ZnO. We attribute these observations to the addition of silver nanoparticles allowing interfacial oxide-to-metal electron transfer within the hybrid Ag/ZnO photocatalyst. The inhibitory and bactericidal activities of samples have been tested against Gram-negative bacteria; *Escherichia coli, Salmonella typhimurium* and gram-positive bacteria; *Staphylococcus aureus, Enterococcus faecium* and *Candida albicans*. The results showed that the Ag/ZnO can be used as photocatalysts and antibacterial agents for potential practical applications in the wastewater treatment.

Graphical Abstract

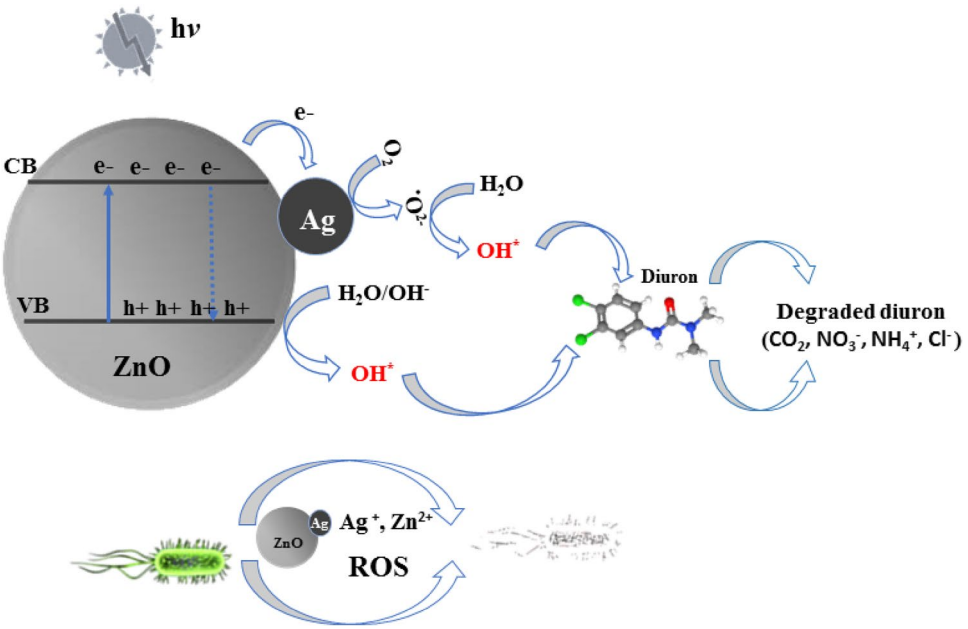

Schematic of the proposed photocatalytic and bactericidal mechanism of Ag/ZnO nanostructure.

Extended author information available on the last page of the article

Keywords ZnO · Ag · Nanoparticles · Photocatalysis · Antibacterial · Wastewater treatment

1 Introduction

Pure-water is known as the source of human life and the most important natural-material in the earth. With the increase in world population, the demand for pure-water was enhanced, indicating a water scarcity problem in the near future. In recent years, on the basis of chemical and physical methodologies, numerous conventional procedures have been developed and used to purify waste water or desalinated sea water [1–3]. Advanced oxidation processes (AOPs) including photocatalysis are one of the most promising techniques in wastewater decontamination areas, they have been utilized to generate the reactive oxygen species (ROS) such as hydroxyl (OH.), superoxide anion ($O_2^{\cdot -}$) radicals and hydrogen peroxide (H_2O_2) for a wide array of pollutant destruction. These highly active radicals participate in oxidation and reduction reactions, micro-organisms inactivation as well as mineralization of pollutants [4–7]. Semiconductor have been broadly studied for this purpose, in particular ZnO have received a great deal of attention because of their thermal and chemical stability, non-toxicity, antibacterial property, and high efficiency for photo-degrading a wide range of dyes, detergents, bacteria and pesticides [8–11]. Yet, ZnO with an important wide-direct band gap (3.37 eV) and a large exciton binding energy (60 meV), is found to be a suitable alternative to TiO_2 and a promising photocatalyst [12, 13]. Furthermore, its higher efficiency than TiO_2 has been found in the photocatalytic oxidation of pulp mill bleaching wastewater, 2-phenylphenol and phenol [14]. Even so, its photoactivity is restricted to ultraviolet irradiation ($\leq$ 387 nm) and still decreased because of photocorrosion effect during light irradiation [15, 16]. In order to extend this restriction into the visible light and then improve photocatalytic activity, combination of ZnO nanostructures with noble metals (Pt, Au and Ag) has been studied [17, 18]. This modification has several advantages, including preventing the recombination of photogenerated electron and hole, broadened the absorption spectrum and facilitated some specific reactions on the surface of ZnO nanostructures [19]. Metallic levels, such as gold, silver and palladium were lower than the conduction band of zinc oxide, so these metals accumulated photogenerated electron upon the ZnO photoexcitation and resulted in an improvement of photocatalytic efficiency [20, 21]. Of the metals, silver represent one of the extensive scientific interest to extend the spectral response of ZnO due to its lower cost than the other noble metals as well as its well-known antibacterial properties that will expand the activities of ZnO materials to a wider variety of applications [22]. Hence, Ag/ZnO structures with various morphologies and sizes have been prepared by several methods such as solvothermal [23], sol–gel [16], seed mediated [24], chemical precipitation [25], polyol [26], microwave [18], ultrasonic irradiation [27] and photo-reduction [28]. For instance, Jin-Chung Sin et al. prepared Ag/ZnO micro/nanoflowers by coprecipitation and photo-deposition routes with enhanced visible light responsive photoactivity towards the degradation of Fast Green dye and inactivation of *Escherichia coli* [29]. Gomathisankar et al. also reported that the bactericidal and photocatalytic activities of microwave synthesized Ag/ZnO, tested, respectively, with *E. coli* and cyanide ion, are larger than those of commercial ZnO nanoparticles [18]. However, it is still a challenge to explore a facile method to synthesize other novel and uniform Ag–ZnO nanostructure with enhanced photocatalytic and bactericidal performance.

In this present work, we report the synthesis, characterization, photocatalytic and antibacterial activity of Ag/ZnO composites prepared by a facile, fast and effective polyol method at low temperature and without any post-synthesis thermal treatment by using only silver (I) and zinc (II) precursors without the addition of any other reagent, template or complex metal ligand. The photocatalytic activity of Ag/ZnO materials has been studied by analyzing the degradation of diuron, under solar light. Diuron, one of the most commonly found herbicide in water ecosystems is considered as highly toxic and persistent with a half-life in soil over 300 days [30]. Malato et al. have proposed a three-step degradation pathway for diuron, together with the identification of the main reaction byproduct [30], in agreement with previous works [31–36]. They explained that the degradation pathway would be first initiated by the attack on the aromatic ring by $OH^{\cdot}$ radicals without dechlorination or alkyl chains. Further, the next step would imply a series of oxidation and decarboxylation processes that eliminates alkyl groups and chlorine atoms, while the last step would presuppose oxidative opening of the aromatic ring, leading to small organic ions and inorganic species. Many studies have been interested by diuron photodegradation using mainly TiO_2-based materials [37–39], but the use of the Ag–ZnO in the photodegradation of diuron has not been reported in the scientific literatures. Moreover, the antibacterial activity of the Ag/ZnO nanostructures has been tested against Gram negative and Gram-positive bacteria that are mainly found in drinking water.

2 Experimental

2.1 Ag/ZnO Nanocomposites Preparation

The synthesis of Ag/ZnO photocatalysts has been carried out via a polyol method in which the polyol solvent plays the role of both complexing and surfactant agent which adsorbs on the nanoparticles surface, thus preventing their agglomeration [40]. All used reagents have been purchased from Sigma Aldrich without further purification. Depending on the materials to be prepared, the precursor solution contained an Ag^{+}/Zn^{2+} molar ratio of 0; 0.7 and 2%. For instance, for 0.7%Ag/ZnO sample, in a 100 ml three-neck round-bottomed flask, 6.8 mmol of zinc acetate dehydrate has been dissolved in 50 ml of triethylene glycol (TEG) with vigorous stirring. The reaction mixture has been heated to 160 °C at the rate of 5 °C/min under magnetic stirring and was kept at this temperature until a white colloidal solution appears indicating the formation of ZnO nanoparticles. At that time 48 µmol of $AgNO_3$ silver salt has been injected into the ZnO suspension and the reaction was pursued at 160 °C up to the change of the solution to a yellow color and then cooled at room temperature. Finally, the powder has been collected using centrifugation, washed several times with ethanol and dried in the stove at 100 °C overnight.

2.2 Characterization

Ag/ZnO photocatalysts have been characterized by X-ray diffraction (XRD) patterns recorded on a Bruker D8 Advance X-ray diffractometer using Cu-K_α radiation ($\lambda = 1.5406$ Å). The mean crystallite size has been calculated using Scherrer's relation. Transmission electron microscopy (TEM, JEOL 2100F) with a point resolution of 0.2 nm has been used to characterize the size and morphology of the products. The Ag content in Ag/ZnO has been determined by inductively coupled plasma optical emission spectroscopy (ICP-OES) carried out on an Optima 7000 DV spectrometer (Perkin Elmer). A UV–Vis spectrophotometer (Varian CARY 100) has been used to record the optical absorption spectra of the samples in the range of 200–800 nm. The Brunauer–Emmett–Teller (BET) surface area measurements have been carried out on a Micrometrics (ASAP 2420) using N_2 as adsorbent at − 196 °C with a prior outgassing at 120 °C overnight.

2.3 Photocatalytic Degradation

Photocatalytic measurements have been carried out in an ATLAS SUNTEST XLS + testing chamber simulating outdoor solar light. This system equipped with a 1700 W, air-cooled Xenon lamps with emission irradiance in the wave length range of 300–800 nm. In a typical photocatalytic experiment, 10 mg of the photocatalyst has been dispersed under stirring in 100 ml diuron solution (10 mg/l) in a beaker-type reactor. After stirring for 2 h in the dark to ensure the adsorption–desorption equilibrium, the suspension has been putting under the solar light irradiation (250 W/m^2) in the appropriate stirring. At regular time intervals, 1 ml of solution has been sampled and then filtered through a 0.20 µm porosity (Chromafil ® PET-20/25) filter to remove the photocatalyst powder if any, before the remaining herbicide concentration has been determined using a UV–Vis spectrophotometer (CARY 100, $\lambda = 248$ nm).

2.4 Testing for Antibacterial Activity

The antibacterial activity of Ag/ZnO photocatalysts has been tested against Gram-negative bacteria; *E. coli* (ATCC 8739) and *Salmonella typhimurium* (ATCC 14028) and gram-positive bacteria; *Staphylococcus aureus* (ATCC 6538), *Enterococcus faecium* (ATCC 19434) and *Candida albicans* (ATCC 10231). The minimum inhibitory concentration (MIC) values have been evaluated through the broth dilution method (NCCLS 2001). Serial dilutions have been performed in 96 well micro plates, 100 µl of each concentration has been pipetted to individual wells and overnight bacterial culture (5×10^6 CFU/ml) on Mueller–Hinton broth (MHB) has been added to each well and incubated for 37 °C for 1 day. After incubation, the progress of inhibition has been observed on the well dishes where the minimum concentration that did not have any turbidity has been taken as MIC. For minimum bactericidal concentrations (MBC), 100 µl of broth medium have been taken from each well which did not show turbidity of the MIC micro plate. These have been spread on sterile Mueller–Hinton Agar (MHA) plates to incubation at 37 °C for 1 day. The lowest concentration of Ag–ZnO has been taken for bacteriological progress on the agar plates and selected for MBC.

3 Results and Discussion

3.1 Powders Characterization

The XRD patterns illustrated in Fig. 1 indicates that the synthesized Ag/ZnO nanocomposites have a good crystallinity and the diffraction peaks have been consistent with the standard hexagonal wurtzite structure of ZnO [space group $P6_3mc$, (a) 3.25 Å, (c) 5.21 Å, JCPDS card no. 36-1451] [41]. Furthermore, three additional small intensity diffraction peaks have been observed at $2\theta = 38.18°$, 44.29° and 64.54° which could be indexed to the (111), (200) and (220)

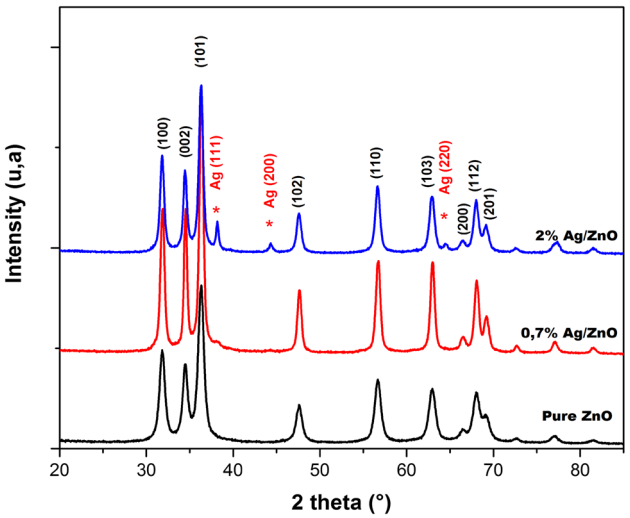

Fig. 1 X-ray diffraction patterns of pure ZnO and Ag/ZnO nanocomposites

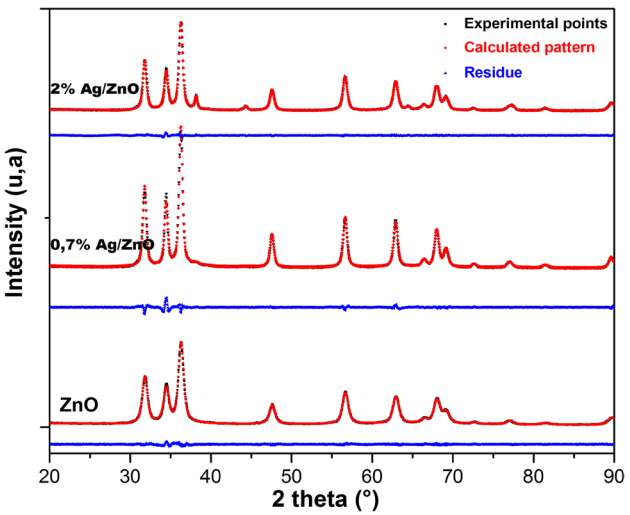

Fig. 2 Profile refinement of pure ZnO and Ag/ZnO powder diffractogram

crystal planes of the face-centered cubic structure of silver metal (space group Fm-3m, JCPDS card no. 04-0783) [42], suggesting that the Ag particles have been modified on the ZnO surface. No characteristic peak has been observed for other impurities such as Zn $(OH)_2$, Ag_2O. The a and c lattice parameters of the hexagonal wurtzite ZnO samples have been refined by the Rietveld method [43] from the XRD patterns using the FULLPROF program (Fig. 2). As shown in Fig. 3, there was a linear increase in the lattice parameters of Ag/ZnO nanoparticles when increasing the molar Ag content, indicating the incorporation of Ag^+ ions into the ZnO lattice sites, probably substituting Zn^{2+} ions. The appearance of Ag peaks in the diffraction patterns clearly indicates the formation of crystalline silver clusters in the nanoparticles. Limited incorporation of Ag + ions into the ZnO lattice through substitution of Zn^{2+} ions was due to their higher ionic radius (1.22 Å) compared to the radius of Zn^{2+} ions (0.74 Å) [15, 44, 45].

The average size of the ZnO crystallites, estimated from the FWHM using Scherrer's relation of the diffraction peaks of ZnO (102), (103) and (110) planes is given in Table 1. It is clear that the addition of silver causes a slight reduction in crystallite size. This phenomenon has already been observed in the case of the cationic substitution of oxide nanomaterials and has been attributed to lower nucleation rates and thus to slower crystallite growth conditions [46, 47].

The molar content of Ag in Ag/ZnO has been measured by ICP-OES at the value of 0%, 0.2% and 0.7% as reported in Table 1. ICP-OES measurements have evidenced that the loading yield of Ag from the precursor salt mixture into the solid remained within the 30% range, in agreement with the chemical analysis of residual Ag in the TEG solvent after synthesis.

Figure 4 shows the absorption spectra Ag/ZnO nanocomposites. The presence of an absorption band in the UV region at about 360 nm which could be attributed to the intrinsic band gap absorption of ZnO clearly exhibited that the materials are photoactive. Furthermore, Ag/ZnO materials displayed an absorption band in the visible region with a maximum absorption wavelength in the range of 410–450 nm, characteristic of Ag nanoparticles plasmon absorption [48]. The band gap of ZnO and the hybrid Ag/ZnO materials have been graphically estimated by Tauc plot method (Fig. 5). For pure ZnO, it has been around 3.22 eV, whilst the band gap of 0.7% and 2% Ag/ZnO samples have been significantly lower. This is due to the size difference in the particles and the substitution of Ag+ ions into the ZnO lattice sites [10, 49].

The morphology and size of as-synthesized ZnO and 2% Ag/ZnO have been investigated by TEM (Fig. 6). The materials have been composed of large quasi-spherical aggregates (300–500 nm) of small-size nanoparticles. By analyzing the ZnO nanoparticles size histograms (Fig. 6 a, d), an average distribution within 15–25 nm range has been observed, in agreement with the mean crystallite size derived from XRD results. Figure 6c indicates the presence of many small Ag particles (blacker particles with size about 50–100 nm) on the surface of the microspheres. Also, we rarely observed free Ag nanoparticles based on analyzing a large number of TEM images, showing the successful combination of Ag NPs with ZnO particles. High magnification images of the 2% Ag/ZnO sample (Fig. 6f) revealed an inter planar spacing of 0.26 nm matched those of the (002) crystallographic plane of ZnO, together with the fringe spacing at 0.24 nm corresponds to the (111) plane of the face-centered cubic phase of AgNPs

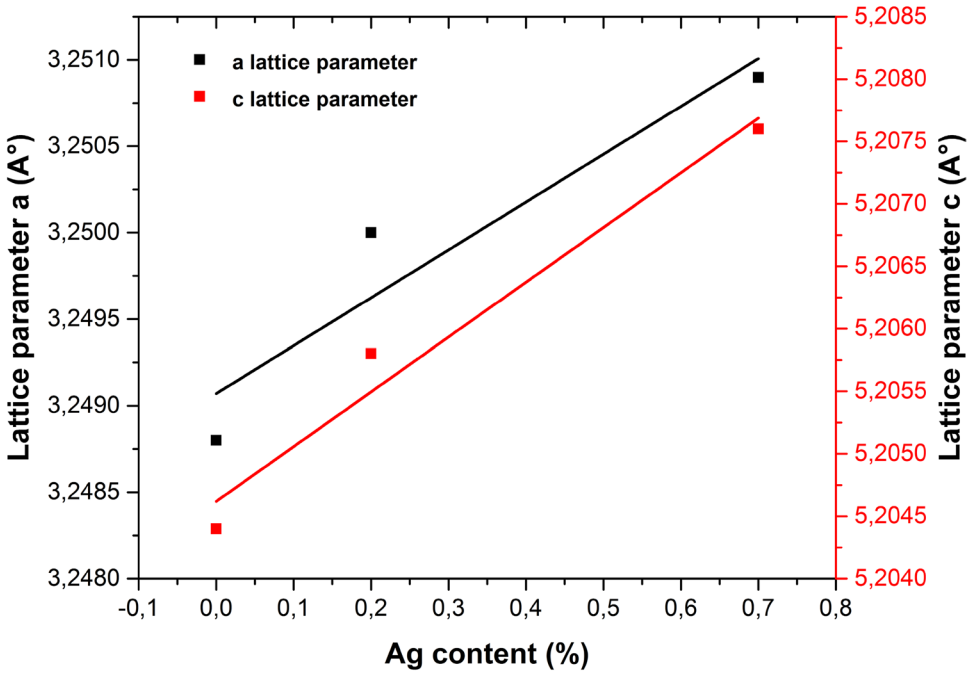

Fig. 3 Influence of the Ag content in Ag/ZnO photocatalysts on both a and c lattice parameters of ZnO

Table 1 Lattice parameters and some properties of Ag/ZnO photocatalysts

Ag content in the synthesis mixture	0.00%	0.7%	2%
Ag content in Ag/ZnO	0.00%	0.2%	0.7%
a (Å)	3.2488 (6)	3.2500 (4)	3.2509 (3)
c (Å)	5.2044 (9)	5.2058 (7)	5.2076 (5)
Cell volume (Å^3)	47.57 (1)	47.62 (1)	47.663 (8)
Average size (nm)	19 ± 1	18 ± 1	16 ± 1
BET surface area (m^2/g)	20.6 (6)	15.0 (1)	14.03 (9)
Band gap (eV)	3.22	3.02	3.11
k (10^{-3} min^{-1})	2.65	37.47	19.03

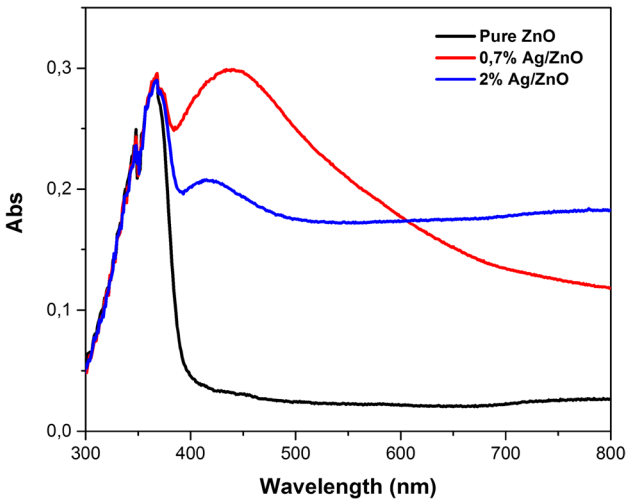

Fig. 4 UV–Vis diffuse reflectance spectra of pure ZnO and Ag/ZnO photocatalysts

[50]. The interference fringes or moiré fringes observed have proposed the presence of a non-coherent ZnO/Ag interface, with a non-epitaxial nucleation and growth of the Ag on the surface of ZnO, as a result of the lattice mismatch between face-centered cubic and hexagonal lattices [40, 51].

Figure 7 shows the nitrogen adsorption–desorption isotherms of Ag/ZnO nanocomposites. The isotherms have the characteristic type IV shape indicating that they are mesoporous materials, with a mainly H_2-type hysteresis behavior characteristic of the presence of interconnected mesopores with non-uniform shape or size. The BET specific surface areas of materials have been summarized in Table 1. It can be seen that the specific surface areas decrease with the Ag addition of 20 m^2/g for pure ZnO to 14 m^2/g for 0.7% Ag/ZnO. These results were in good agreement with the decrease in the ZnO mean crystallite size derived from XRD.

3.2 Photocatalytic Activity

The photocatalytic performance has been evaluated by the degradation of the most commonly used organic herbicide diuron, in aqueous solution, under simulated solar light irradiation at room temperature with a photocatalyst concentration of 10 mg/100 ml. The photocatalytic degradation kinetics of the organic pollutant has been modeled using a

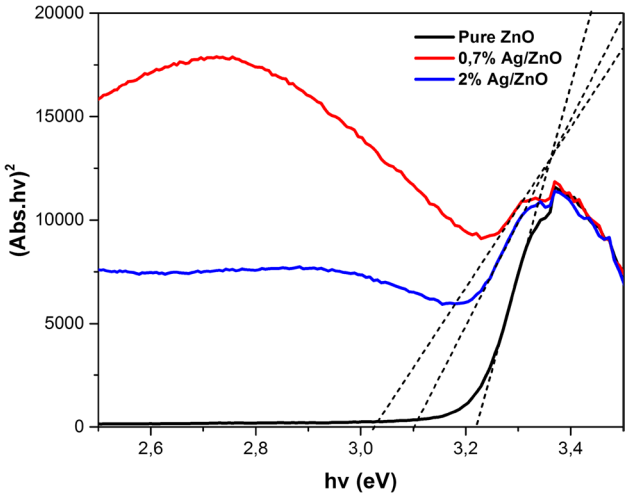

Fig. 5 Tauc plot for the absorption spectra of pure ZnO and Ag/ZnO photocatalysts

pseudo-first order equation with $\ln(C_0/C_t) = k_{app}(t)$ for highly diluted solutions, C_0 and C_t being the initial and instantaneous diuron concentrations, respectively, and k_{app} being the apparent rate constant. The rate constant of bare ZnO has been calculated as a reference to compare with that of the Ag/ZnO catalysts.

At first, the concentration of diuron has no obvious change in the presence of the bare and hybrids ZnO photocatalysts under dark conditions. Also, no detectable degradation of diuron has been observed after 10 h under simulated solar light and without using any catalysts, revealing that the direct photolysis of the herbicide can be ignored in the experiment, as reported by El Madani et al. [52] and Quinones et al. [53]. However, the results evidenced that the photodegradation of diuron has been greatly improved by the modification of zinc oxide nanoparticles with low amount of silver. 0.7% Ag/ZnO exhibited the best photocatalytic activity for the degradation of diuron under solar light with which the maximum absorbance peak of the diuron (at about 248 nm) decreased gradually and disappeared after 90 min, indicating that the herbicide has been degraded entirely (Fig. 8). The surface modification of ZnO with Ag nanoparticles was strongly favorable to the kinetic rate constant, that increased 14 times from 2.65×10^{-3} min^{-1} for the pure ZnO to 37.47×10^{-3} min^{-1} for 0.7% Ag/ZnO (Fig. 9).

The loading of Ag nanoparticles with the appropriate amount on ZnO surface can effectively capture and transfer the photogenerated electrons, and thus inhibit their combination of the electron–hole pairs. However, more Ag salt has been used, the aggregation and/or size increase of the Ag particles will happen, so that photogenerated charge carriers recombine more easily. On the other hand, the decrease in photocatalytic activity at higher Ag contents is considered to be related to the increased absorbing and scattering of photons by Ag in the photoreaction system. These results agree well with those obtained previously using Ag/ZnO for the photodegradation of methylene blue [54] and Rhodamine B [23].

In general, the efficiency and operating mechanism of photodegradation are different depending on whether excitation wavelength (UV or visible light) occurs on the semiconductor (metallic nanoparticles acting as electron buffer and site for gas generation) or on the surface

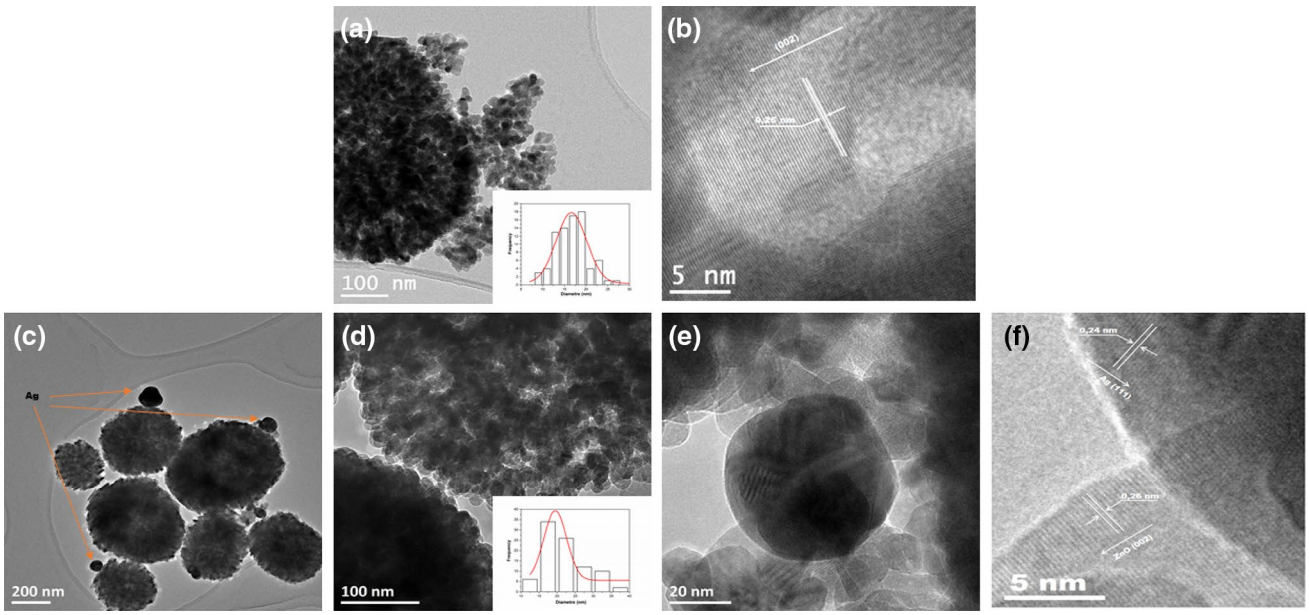

Fig. 6 **a, b** TEM and HRTEM images of pure ZnO. **c–f** TEM and HRTEM images of 2% Ag/ZnO

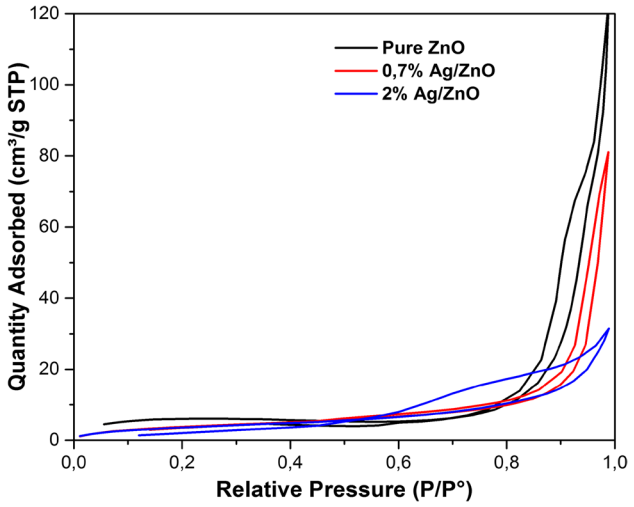

Fig. 7 N2 adsorption–desorption isotherms of pure ZnO and Ag/ZnO photocatalysts

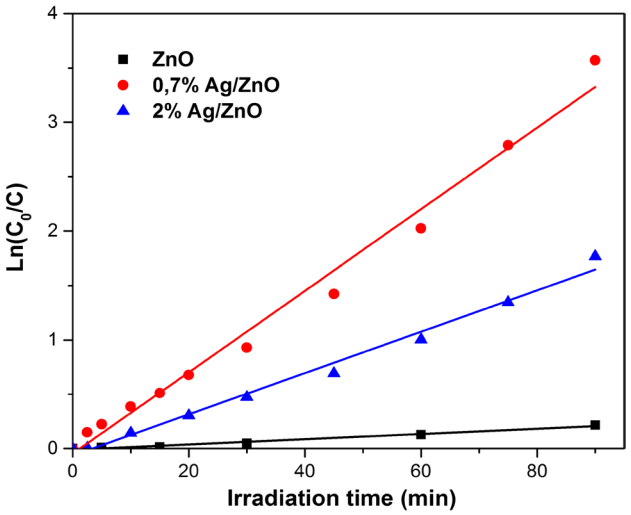

Fig. 9 Ln(C_0/C) versus irradiation time for the degradation of diuron under simulated solar light on Ag/ZnO photocatalysts

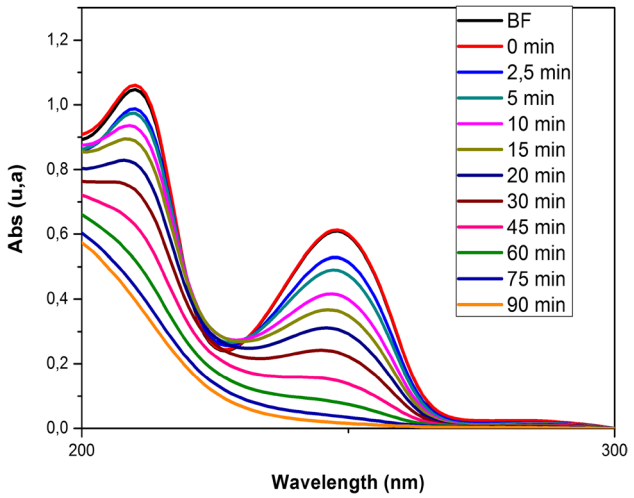

Fig. 8 The absorbance spectra of diuron aqueous solution in the presence of 0.7% Ag/ZnO nanocomposit after different irradiation time

plasmon band of metal (photo-injection of electrons from metal onto the semiconductor conduction band) [21, 55, 56]. In our conditions, and in agreement with the previous studies for the degradation of organic species under solar light using metal–semiconductor photocatalysts, the significant enhancement of the degradation rate results from strongly increased performances towards the UV-A part of the whole solar light spectra [20, 57–59]. When the solar light was irradiated on the Ag/ZnO surface, the e^- in the valence band of ZnO can be photogenerated, leaving h^+. The newly formed Fermi level of Ag/ZnO photocatalysts being lower than the energy of the bottom of the conduction band (Fermi level of Ag 0.99 eV vs. NHE) [60], the direct photoexcitation of the ZnO makes possible the transfer of photogenerated e^- from the conduction band into Ag nanoparticles, where it is trapped by electron acceptors such as adsorbed O_2 to produce superoxide radical anions ($O_2^{\cdot -}$). Then, the $O_2^{\cdot -}$ radicals can further react with H_2O to produce H_2O_2 in aqueous solution. Further, H_2O_2 reacts with electrons to form $OH^{\cdot}$ radicals. At the same time, photogenerated holes (h^+) react with water molecules to generate $OH^{\cdot}$ radicals. Therefore, $OH^{\cdot}$ radicals are responsible for degradation of diuron herbicide (Scheme 1).

The photo-stability of 0.7% Ag/ZnO nanocomposite as photocatalyst under solar light has also been studied (Fig. 10). It can be seen that the photocatalytic activity of the composite did not decrease conspicuously after five successive cycles of degradation tests. Moreover, we also examined the 0.7% Ag/ZnO sample after the fifth cycle using UV–Vis spectroscopy. The UV–Vis spectrum was similar to the initial spectrum. These results highlight the stability and reusability of the Ag/ZnO nanocomposites.

The photodegradation of diuron in aqueous solution has been the subject of further investigation, for instance, TiO_2 doped with Samarium [61] and tungsten [38] have been synthesized via sol gel method followed by calcination for successfully diuron sunlight degradation. Both this photocatalysts showed low photocatalytic performance than the us prepared Ag/ZnO especially when compared to its height concentration in the photocatalytic degradation procedure. Therefore, based on their excellent photocatalytic performance and its simple synthesis method without any post-synthesis thermal treatment the Ag/ZnO photocatalyst are possibly favorable for potential application in the purification of polluted water.

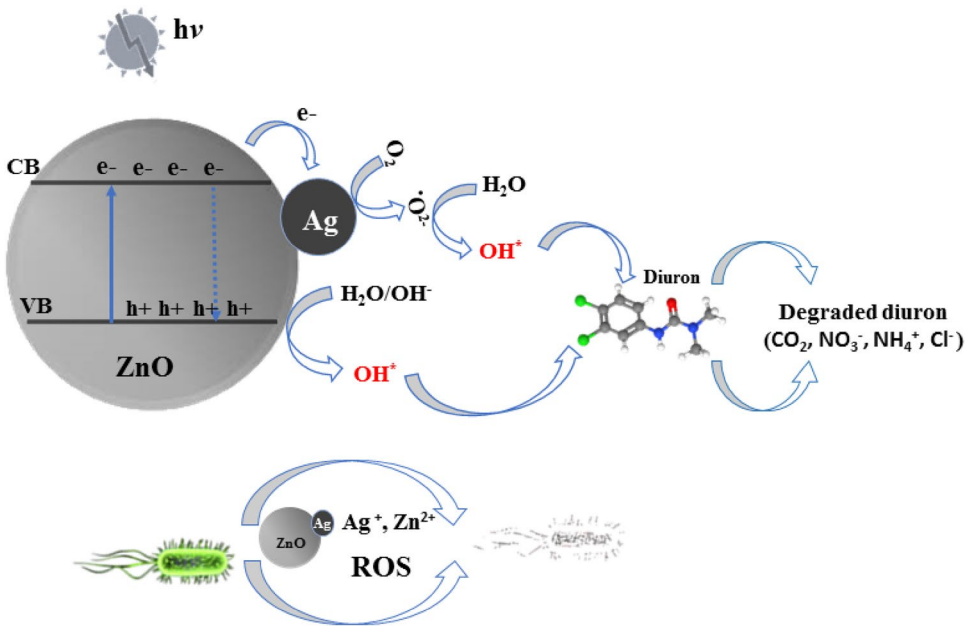

Scheme 1 Schematic of the proposed photocatalytic and bactericidal mechanism of Ag/ZnO nanostructure

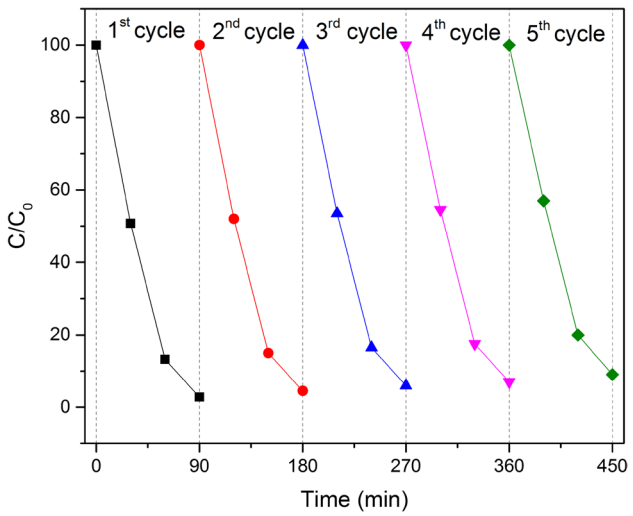

Fig. 10 Cycling runs in the photodegradation of diuron in the presence of 0.7% Ag/ZnO nanocomposite under solar light irradiation

3.3 Antibacterial Activity

The MIC, MCB and MBC/MIC ratios values of the Ag/ZnO photocatalysts against both Gram-negative (G−) *E. coli, S. typhimurium* and Gram-positive (G+) *S. aureus, E. faecium, C. albicans* bacteria have been shown in Table 2 and Fig. 11. A lower MIC value indicates a better antimicrobial agent as less compound is required to inhibit growth of the bacteria. Preliminary results showed that all the prepared materials have been effective in inhibiting the growth of all tested bacteria with MIC values in the range of 0.0625–0.500 mg/ml. An antimicrobial agent is considered bactericidal if the MBC is not more than four-fold higher than the MIC [62, 63]. All the prepared materials have been shown to be bactericidal (MBC/MIC ≤ 4) towards both Gram-positive and Gram-negative strains.

The MIC values of the prepared Ag/ZnO at Ag 0.7% contents were 0.250 g/ml for *E. coli* (G−) and 0.125 g/ml for *S. aureus* (G+). These values are better than those previously reported by Lu et al. (MIC = 0.600 g/ml for *E. coli* and 0.400 g/ml for *S. aureus*) [64] and Amornpitoksuk et al. (MIC = 0.512 mg/ml for *E. coli* and 0.256 mg/ml for *S. aureus*) [65]. The antibacterial activity of 0.7% Ag/ZnO is larger than pure ZnO catalyst, especially against gram-positive *S. aureus* and *C. albicans* known worldwide as toxigenic bacteria which are considered a dangerous threat to human life [66–69]. However, pure ZnO was more potent than Ag/ZnO against Gram-negative *E. coli* and *S. typhimurium* bacteria at low concentration (MIC = 0.125 mg/ml). The 0.7% Ag–ZnO shows a much stronger antibacterial activity on Gram-positive than on Gram-negative bacteria. The difference in activity against these two types of bacteria is commonly reported in the literature and it can be explained by the different structures and chemical composition of the cell surfaces [65, 70].

The bactericidal activity of Ag/ZnO can be attributed to the released Ag^+ from Ag nanoparticles and released Zn^{2+} from ZnO nanostructures, that harm the bacterial cells [71–73]. In addition, reactive oxygen species (ROS) can be further another way for the antibacterial efficiency under dark conditions. This fact is attributed to the oxygen defects from the surface of ZnO nanostructures. This mechanism was fully consistent with previous works [74–76].

Table 2 Minimum inhibitory concentrations (MIC) and bactericidal (MBC) and their ratio of Ag/ZnO

	ZnO			0.7% Ag/ZnO			2% Ag/ZnO		
	MIC (mg/ml)	MBC (mg/ml)	MBC/MIC ratio	MIC (mg/ml)	MBC (mg/ml)	MBC/MIC ratio	MIC (mg/ml)	MBC (mg/ml)	MBC/MIC ratio
Escherichia coli	0.125	0.250	2	0.250	0.500	2	0.250	0.500	2
Salmonella typhimurium	0.125	0.250	2	0.500	0.500	1	0.125	0.125	1
Staphylococcus aureus	0.250	0.500	2	0.125	0.500	4	0.250	1	4
Enterococcus faecium	0.0625	0.125	2	0.0625	0.250	4	0.125	0.250	2
Candida albicans	0.125	0.250	2	0.0625	0.250	4	0.125	0.500	4

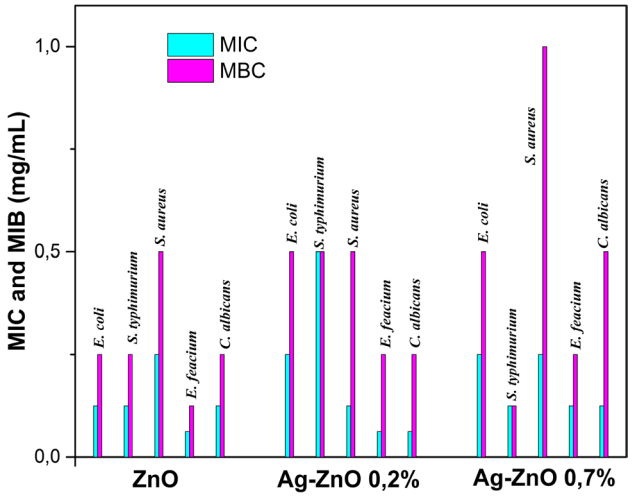

Fig. 11 Evolution of minimum inhibitory concentrations (MIC) and bactericidal (MBC)

4 Conclusion

Ag/ZnO photocatalysts have been successfully prepared via a facile, fast and effective polyol method at low-temperature and without any post-synthesis thermal treatment by using only silver (I) and zinc (II) precursors without the addition of any other reagent, template or complex metal ligand. Photocatalytic activity was evaluated using diuron herbicide as a model contaminant under simulated solar light irradiation. The results of photocatalytic experiments indicated that the loading of Ag nanoparticles with appropriate amount on ZnO surface exhibited superior photocatalytic performance than pure ZnO and the herbicide molecule has been degraded entirely after 90 min of solar irradiation. However, the pseudo first-order rate constant in Ag/ZnO with 0.7% Ag molar content photocatalytic process (37.4710^{-3} min^{-1}) was about 14 times for bare ZnO (2.6510^{-3} min^{-1}). Also, the Ag/ZnO samples displayed superior antibacterial ability against both Gram-negative bacteria; *E. coli, S. typhimurium* and gram-positive bacteria; *S. aureus, E. faecium* and *C. albicans*. All the prepared materials have been shown to be bactericidal (MBC/MIC ≤ 4) towards both Gram-positive and Gram-negative strains. Therefore, these materials can be the base for the development of industrial application of the photocatalysis on wastewater treatment.

Acknowledgements Mohamed Ali Saidani gratefully acknowledges the support of the Ministry of Higher Education and Scientific Research of Tunisia. The French National Research Agency is gratefully acknowledged for partial funding of this work, University of Strasbourg, ICPEES are thanked for technical support.

References

1. G. Chen, Electrochemical technologies in wastewater treatment. Sep. Purif. Technol. **38**, 11–41 (2004)
2. P.R. Gogate, A.B. Pandit, A review of imperative technologies for wastewater treatment I: oxidation technologies at ambient conditions. Adv. Environ. Res. **8**, 501–551 (2004)
3. A.D. Khawaji, I.K. Kutubkhanah, J.-M. Wie, Advances in seawater desalination technologies. Desalination **221**, 47–69 (2008)
4. B. Roig, C. Gonzalez, O. Thomas, Monitoring of phenol photodegradation by ultraviolet spectroscopy. Spectrochim Acta A **59**, 303–307 (2003)
5. K. Vignesh, A. Suganthi, M. Rajarajan, S.A. Sara, Photocatalytic activity of AgI sensitized ZnO nanoparticles under visible light irradiation. Powder Technol. **224**, 331–337 (2012)
6. S. Giannakis, M. Jovic, N. Gasilova, M. Pastor Gelabert, S. Schindelholz, J.-M. Furbringer, H. Girault, C. Pulgarin, Iohexol degradation in wastewater and urine by UV-based advanced oxidation processes (AOPs): process modeling and by-products identification. J. Environ. Manag. **195**, 174–185 (2017)
7. M. Cheng, G. Zeng, D. Huang, C. Lai, P. Xu, C. Zhang, Y. Liu, Hydroxyl radicals based advanced oxidation processes (AOPs) for remediation of soils contaminated with organic compounds: a review. Chem. Eng. J. **284**, 582–598 (2016)
8. S. Navarro, J. Fenoll, N. Vela, E. Ruiz, G. Navarro, Photocatalytic degradation of eight pesticides in leaching water by use of ZnO under natural sunlight. J. Hazard. Mater. **172**, 1303–1310 (2009)
9. L.-H. Li, J.-C. Deng, H.-R. Deng, Z.-L. Liu, X.-L. Li, Preparation, characterization and antimicrobial activities of chitosan/Ag/ZnO blend films. Chem. Eng. J. **160**, 378–382 (2010)
10. M.J. Height, S.E. Pratsinis, O. Mekasuwandumrong, P. Praserthdam, Ag-ZnO catalysts for UV-photodegradation of methylene blue. Appl. Catal. B **63**, 305–312 (2006)
11. C. Hariharan, Photocatalytic degradation of organic contaminants in water by ZnO nanoparticles: Revisited. Appl. Catal. A **304**, 55–61 (2006)

12. N. Daneshvar, D. Salari, A.R. Khataee, Photocatalytic degradation of azo dye acid red 14 in water on ZnO as an alternative catalyst to TiO_2. J Photochem. Photobiol. A **162**, 317–322 (2004)
13. A. Mills, S. LeHunte, An overview of semiconductor photocatalysis. J. Photochem. Photobiol. A **108**, 1–35 (1997)
14. N. Sobana, M. Swaminathan, The effect of operational parameters on the photocatalytic degradation of acid red 18 by ZnO. Sep. Purif. Technol. **56**, 101–107 (2007)
15. M. Ahmad, E. Ahmed, Z.L. Hong, N.R. Khalid, W. Ahmed, A. Elhissi, Graphene–Ag/ZnO nanocomposites as high performance photocatalysts under visible light irradiation. J. Alloy. Compd. **577**, 717–727 (2013)
16. R. Georgekutty, M.K. Seery, S.C. Pillai, A highly efficient Ag-ZnO photocatalyst: synthesis, properties, and mechanism. J. Phys. Chem. C **112**, 13563–13570 (2008)
17. S. Pearton, Amino acid-assisted one-pot assembly of Au, Pt nanoparticles onto one-dimensional ZnO microrods. Nanoscale **2**, 1057 (2010)
18. C. Karunakaran, V. Rajeswari, P. Gomathisankar, Optical, electrical, photocatalytic, and bactericidal properties of microwave synthesized nanocrystalline Ag–ZnO and ZnO. Solid State Sci. **13**, 923–928 (2011)
19. R.S. Patil, M.R. Kokate, D.V. Shinde, S.S. Kolekar, S.H. Han, Synthesis and enhancement of photocatalytic activities of ZnO by silver nanoparticles. Spectrochim. Acta A **122**, 113–117 (2014)
20. J. Lee, H.S. Shim, M. Lee, J.K. Song, D. Lee, Size-controlled electron transfer and photocatalytic activity of ZnO–Au nanoparticle composites. J. Phys. Chem. Lett. **2**, 2840–2845 (2011)
21. Q. Deng, X. Duan, D.H. Ng, H. Tang, Y. Yang, M. Kong, Z. Wu, W. Cai, G. Wang, Ag nanoparticle decorated nanoporous ZnO microrods and their enhanced photocatalytic activities. ACS Appl. Mater. Interfaces **4**, 6030–6037 (2012)
22. Y. Zhang, X. Gao, L. Zhi, X. Liu, W. Jiang, Y. Sun, J. Yang, The synergetic antibacterial activity of Ag islands on ZnO (Ag/ZnO) heterostructure nanoparticles and its mode of action. J. Inorg. Biochem. **130**, 74–83 (2014)
23. B. Chai, X. Wang, S. Cheng, H. Zhou, F. Zhang, One-pot triethanolamine-assisted hydrothermal synthesis of Ag/ZnO heterostructure microspheres with enhanced photocatalytic activity. Ceram. Int. **40**, 429–435 (2014)
24. X. Yin, W. Que, D. Fei, F. Shen, Q. Guo, Ag nanoparticle/ZnO nanorods nanocomposites derived by a seed-mediated method and their photocatalytic properties. J. Alloy. Compd. **524**, 13–21 (2012)
25. R. Chauhan, A. Kumar, R.P. Chaudhary, Photocatalytic studies of silver doped ZnO nanoparticles synthesized by chemical precipitation method. J. Sol-Gel. Sci. Technol. **63**, 546–553 (2012)
26. C. Tian, W. Li, K. Pan, Q. Zhang, G. Tian, W. Zhou, H. Fu, One pot synthesis of Ag nanoparticle modified ZnO microspheres in ethylene glycol medium and their enhanced photocatalytic performance. J. Solid State Chem. **183**, 2720–2725 (2010)
27. Y. Zhu, D. Liu, Y. Lai, M. Meng, Ambient ultrasonic-assisted synthesis, stepwise growth mechanisms, and photocatalytic activity of flower-like nanostructured ZnO and Ag/ZnO. J. Nanoparticle Res. **16**(3), 2305 (2014)
28. T. Alammar, A.-V. Mudring, Facile preparation of Ag/ZnO nanoparticles via photoreduction. J. Mater. Sci. **44**, 3218–3222 (2009)
29. S.-M. Lam, J.-A. Quek, J.-C. Sin, Mechanistic investigation of visible light responsive Ag/ZnO micro/nanoflowers for enhanced photocatalytic performance and antibacterial activity. J. Photochem. Photobiol. A **353**, 171–184 (2018)
30. S. Malato, J. Caceres, A.R. Fernandez-Alba, L. Piedra, M.D. Hernando, A. Aguera, J. Vial, Photocatalytic treatment of diuron by solar photocatalysis: evaluation of main intermediates and toxicity. Environ. Sci. Technol. **37**, 2516–2524 (2003)
31. E. Pramauro, M. Vincenti, V. Augugliaro, L. Palmisano, Photocatalytic degradation of monuron in aqueous titanium dioxide dispersions. Environ. Sci. Technol. **27**, 1790–1795 (1993)
32. J. Jirkovský, V. Faure, P. Boule, Photolysis of diuron. Pestic. Sci. **50**, 42–52 (1997)
33. P. Mazellier, B. Sulzberger, Diuron degradation in irradiated, heterogeneous iron/oxalate systems: the rate-determining step. Environ. Sci. Technol. **35**, 3314–3320 (2001)
34. E. Vulliet, C. Emmelin, J.-M. Chovelon, C. Guillard, J.-M. Herrmann, Photocatalytic degradation of sulfonylurea herbicides in aqueous TiO_2. Appl. Catal. B **38**, 127–137 (2002)
35. L. Amir Tahmasseb, S. Nélieu, L. Kerhoas, J. Einhorn, Ozonation of chlorophenylurea pesticides in water: reaction monitoring and degradation pathways. Sci. Total Environ. **291**, 33–44 (2002)
36. H. Katsumata, M. Sada, Y. Nakaoka, S. Kaneco, T. Suzuki, K. Ohta, Photocatalytic degradation of diuron in aqueous solution by platinized TiO_2. J. Hazard. Mater. **171**, 1081–1087 (2009)
37. M. Carrier, C. Guillard, M. Besson, C. Bordes, H. Chermette, Photocatalytic degradation of diuron: experimental analyses and simulation of HO degrees radical attacks by density functional theory calculations. J. Phys. Chem. A **113**, 6365–6374 (2009)
38. G. Foura, A. Soualah, D. Robert, Effect of W doping level on TiO_2 on the photocatalytic degradation of diuron. Water Sci. Technol. **75**, 20–27 (2017)
39. A. Mezni, N.B. Saber, M.M. Ibrahim, M. El-Kemary, A. Aldalbahi, P. Feng, L. Samia, T. Smiri, Altalhi, Facile synthesis of highly thermally stable TiO_2 photocatalysts. New J. Chem. **41**, 5021–5027 (2017)
40. A. Mezni, A. Mlayah, V. Serin, L.S. Smiri, Synthesis of hybrid Au–ZnO nanoparticles using a one pot polyol process. Mater. Chem. Phys. **147**, 496–503 (2014)
41. L. Li, X. Zhang, W. Zhang, L. Wang, X. Chen, Y. Gao, Microwave-assisted synthesis of nanocomposite Ag/ZnO–TiO_2 and photocatalytic degradation Rhodamine B with different modes. Colloids Surf. A **457**, 134–141 (2014)
42. S.A. Ansari, M.M. Khan, J. Lee, M.H. Cho, Highly visible light active Ag@ZnO nanocomposites synthesized by gel-combustion route. J. Ind. Eng. Chem. **20**, 1602–1607 (2014)
43. H.M. Rietveld, Line profiles of neutron powder diffraction peaks for structure refinement. J. Appl. Crystallogr. **22**(1), 151–152 (1967)
44. H.S. Kang, B.D. Ahn, J.H. Kim, G.H. Kim, S.H. Lim, H.W. Chang, S.Y. Lee, Structural, electrical, and optical properties of p-type ZnO thin films with Ag dopant. Appl. Phys. Lett. **88**, 202108 (2006)
45. R.D. Shannon, Revised effective ionic radii and systematic studies of interatomic distances in halides and chalcogonides. Acta Crystallogr. 32(5), 751–767 (1976)
46. J. Hays, A. Punnoose, R. Baldner, M.H. Engelhard, J. Peloquin, K.M. Reddy, Relationship between the structural and magnetic properties of Co-doped SnO_2 nanoparticles, Phys. Rev. B 72(7), 72 (2005)
47. H. Liang, J.M. Raitano, G. He, A.J. Akey, I.P. Herman, L. Zhang, S.-W. Chan, Aqueous co-precipitation of Pd-doped cerium oxide nanoparticles: chemistry, structure, and particle growth. J. Mater. Sci. **47**, 299–307 (2011)
48. T.H. Benjamin, Y. Wiley, Sun, Y. Xia, Polyol synthesis of silver nanoparticles: use of chloride and oxygen to promote the formation of single-crystal, truncated cubes and tetrahedrons. Nano Lett. **4**, 1733–1739 (2004)
49. S.H. Jeong, B.N. Park, S.B. Lee, J.H. Boo, Structural and optical properties of silver-doped zinc oxide sputtered films. Surf. Coat. Technol. **193**, 340–344 (2005)
50. H. Mou, C. Song, Y. Zhou, B. Zhang, D. Wang, Design and synthesis of porous Ag/ZnO nanosheets assemblies as super

photocatalysts for enhanced visible-light degradation of 4-nitrophenol and hydrogen evolution. Appl. Catal. B **221**, 565–573 (2018)
51. D.B. Williams, C.B. Carter, *Transmission Electron Microscopy: A Textbook for Materials Science* (Plenum Press, New York, 1996), pp. 441–455
52. M.E. Madani, C. Guillard, N. Pérol, J.M. Chovelon, M.E. Azzouzi, A. Zrineh, J.M. Herrmann, Photocatalytic degradation of diuron in aqueous solution in presence of two industrial titania catalysts, either as suspended powders or deposited on flexible industrial photoresistant papers. Appl. Catal. B **65**, 70–76 (2006)
53. D.H. Quiñones, A. Rey, P.M. Álvarez, F.J. Beltrán, G.L. Puma, Boron doped TiO_2 catalysts for photocatalytic ozonation of aqueous mixtures of common pesticides: diuron, o-phenylphenol, MCPA and terbuthylazine. Appl. Catal. B **178**, 74–81 (2015)
54. Z. Zhang, H. Liu, H. Zhang, H. Dong, X. Liu, H. Jia, B. Xu, Synthesis of spindle-like Ag/ZnO heterostructure composites with enhanced photocatalytic performance. Superlattices Microstruct. **65**, 134–145 (2014)
55. M. Misra, P. Kapur, M.K. Nayak, M. Singla, Synthesis and visible photocatalytic activities of a Au@Ag@ZnO triple layer core–shell nanostructure. New J. Chem. **38**, 4197–4203 (2014)
56. A. Primo, A. Corma, H. Garcia, Titania supported gold nanoparticles as photocatalyst. Phys. Chem. Chem. Phys. **13**, 886–910 (2011)
57. A. Fkiri, M.R. Santacruz, A. Mezni, L.S. Smiri, V. Keller, N. Keller, One-pot synthesis of lightly doped $Zn_{1-x}Cu_xO$ and Au–$Zn_{1-x}Cu_xO$ with solar light photocatalytic activity in liquid phase. Environ. Sci. Pollut. Res. Int. **24**, 15622–15633 (2017)
58. N.L. Gavade, S.B. Babar, A.N. Kadam, A.D. Gophane, K.M. Garadkar, Fabrication of M@CuxO/ZnO (M = Ag, Au) heterostructured nanocomposite with enhanced photocatalytic performance under sunlight. Ind. Eng. Chem. Res. **56**, 14489–14501 (2017)
59. S. Kaviya, E. Prasad, Biogenic synthesis of ZnO–Ag nano custard apples for efficient photocatalytic degradation of methylene blue by sunlight irradiation. RSC Adv. **5**, 17179–17185 (2015)
60. Q. Zhu, X. Hu, M.S. Stanislaus, N. Zhang, R. Xiao, N. Liu, Y. Yang, A novel P/Ag/Ag_2O/Ag_3PO_4/TiO_2 composite film for water purification and antibacterial application under solar light irradiation. Sci. Total Environ. **577**, 236–244 (2017)
61. D. de la Cruz, J.C. Arevalo, G. Torres, R.G.B. Margulis, C. Ornelas, A. Aguilar-Elguezabal, TiO2 doped with Sm^{3+} by sol-gel: synthesis, characterization and photocatalytic activity of diuron under solar light. Catal. Today **166**, 152–158 (2011)
62. M.E. Levison, Pharmacodynamics of antimicrobial drugs. Infect Dis. Clin. N. Am. **18**, 451–465, vii (2004)
63. J.-H. Sim, N.S. Jamaludin, C.-H. Khoo, Y.-K. Cheah, S.N.B.A. Halim, H.-L. Seng, E.R.T. Tiekink, In vitro antibacterial and time-kill evaluation of phosphanegold(I) dithiocarbamates, $R_3PAu[S_2CN(iPr)CH_2CH_2OH]$ for R=Ph, Cy and Et, against a broad range of Gram-positive and Gram-negative bacteria. Gold Bull. **47**, 225–236 (2014)
64. W. Lu, G. Liu, S. Gao, S. Xing, J. Wang, Tyrosine-assisted preparation of Ag/ZnO nanocomposites with enhanced photocatalytic performance and synergistic antibacterial activities. Nanotechnology **19**, 445711 (2008)
65. P. Amornpitoksuk, S. Suwanboon, S. Sangkanu, A. Sukhoom, N. Muensit, J. Baltrusaitis, Synthesis, characterization, photocatalytic and antibacterial activities of Ag-doped ZnO powders modified with a diblock copolymer. Powder Technol. **219**, 158–164 (2012)
66. G. Gonzalez-Aspajo, H. Belkhelfa, L. Haddioui-Hbabi, G. Bourdy, E. Deharo, Sacha Inchi Oil (*Plukenetia volubilis* L.), effect on adherence of *Staphylococus aureus* to human skin explant and keratinocytes in vitro. J. Ethnopharmacol. **171**, 330–334 (2015)
67. S.T. Omara, MIC and MBC of honey and gold nanoparticles against methicillin-resistant (MRSA) and vancomycin-resistant (VRSA) coagulase-positive *S. aureus* isolated from contagious bovine clinical mastitis. J. Genet. Eng. Biotechnol. **15**, 219–230 (2017)
68. K. Iwata, Toxins produced by *Candida albicans*. Contrib Microbiol Immunol. **4**, 77–85 (1977)
69. M.J. McCullough, B.C. Ross, P.C. Reade, Candida albicans: a review of its history, taxonomy, epidemiology, virulence attributes, and methods of strain differentiation. Int. J. Oral Maxillofac. Surg. **25**, 136–144 (1996)
70. M. Fang, J.-H. Chen, X.-L. Xu, P.-H. Yang, H.F. Hildebrand, Antibacterial activities of inorganic agents on six bacteria associated with oral infections by two susceptibility tests. Int. J. Antimicrob. Agents **27**, 513–517 (2006)
71. Y. Qin, C. Zhu, J. Chen, Y. Chen, C. Zhang, The absorption and release of silver and zinc ions by chitosan fibers. J. Appl. Polym. Sci. **101**, 766–771 (2006)
72. V.K. Sharma, R.A. Yngard, Y. Lin, Silver nanoparticles: green synthesis and their antimicrobial activities. Adv. Colloid Interface Sci. **145**, 83–96 (2009)
73. X. Wang, Y. Du, J. Yang, Y. Tang, J. Luo, Preparation, characterization, and antimicrobial activity of quaternized chitosan/organic montmorillonite nanocomposites. J. Biomed. Mater. Res. A **84**, 384–390 (2008)
74. K. Hirota, M. Sugimoto, M. Kato, K. Tsukagoshi, T. Tanigawa, H. Sugimoto, Preparation of zinc oxide ceramics with a sustainable antibacterial activity under dark conditions. Ceram. Int. **36**, 497–506 (2010)
75. V. Lakshmi Prasanna, R. Vijayaraghavan, Insight into the mechanism of antibacterial activity of ZnO: surface defects mediated reactive oxygen species even in the dark. Langmuir **31**, 9155–9162 (2015)
76. J.M. Wu, W.T. Kao, Heterojunction nanowires of $Ag_xZn_{1-x}O$–ZnO photocatalytic and antibacterial activities under visible-light and dark conditions. J. Phys. Chem. C **119**, 1433–1441 (2015)

Affiliations

Mohamed Ali Saidani[1] · Anis Fkiri[1] · Leila-Samia Smiri[1]

✉ Mohamed Ali Saidani
mohamedali1622@gmail.com

[1] Unité de Recherche Synthèse et Structure de Nanomatériaux UR11 ES30, Faculté des Sciences de Bizerte, Université de Carthage, 7021 Jarzouna, Bizerte, Tunisia